



Article

Ab Initio Study of the Interaction of a Graphene Surface Decorated with a Metal-Doped C₃₀ with Carbon Monoxide, Carbon Dioxide, Methane, and Ozone

Mónica Canales ¹, Juan Manuel Ramírez-de-Arellano ^{2,*}, Juan Salvador Arellano ¹
and Luis Fernando Magaña ^{3,*}

- ¹ Universidad Autónoma Metropolitana Unidad Azcapotzalco, Av. San Pablo Xalpa No. 180, Colonia Reynosa Tamaulipas, Delegación Azcapotzalco, Ciudad de México 02200, Mexico; monic.canales@gmail.com (M.C.); jsap@azc.uam.mx (J.S.A.)
- ² Escuela de Ingeniería y Ciencias, Tecnológico de Monterrey, Av. Eugenio Garza Sada 2501, Monterrey 64849, Mexico
- ³ Instituto de Física, Universidad Nacional Autónoma de México, Apartado Postal 20-364, Ciudad de México 01000, Mexico
- * Correspondence: jramirezdearellano@tec.mx (J.M.R.-d.-A.); fernando@fisica.unam.mx (L.F.M.)

Abstract: Using DFT simulations, we studied the interaction of a semifullerene C₃₀ and a defected graphene layer. We obtained the C₃₀ chemisorbs on the surface. We also found the adsorbed C₃₀ chemisorbs, Li, Ti, or Pt, on its concave part. Thus, the resulting system (C₃₀-graphene) is a graphene layer decorated with a metal-doped C₃₀. The adsorption of the molecules depends on the shape of the base of the semifullerene and the dopant metal. The CO molecule adsorbed without dissociation in all cases. When the bottom is a pentagon, the adsorption occurs only with Ti as the dopant. It also adsorbs for a hexagon as the bottom with Pt as the dopant. The carbon dioxide molecule adsorbs in the two cases of base shape but only when lithium is the dopant. The adsorption occurs without dissociation. The ozone molecule adsorbs on both surfaces. When Ti or Pt are dopants, we found that the O₃ molecule always dissociates into an oxygen molecule and an oxygen atom. When Li is the dopant, the O₃ molecule adsorbs without dissociation. Methane did not adsorb in any case. Calculating the recovery time at 300 K, we found that the system may be a sensor in several instances.

Keywords: carbon nanostructures; semifullerene; pollutant molecules; adsorption; graphene; carbon monoxide; carbon dioxide; methane; ozone



Citation: Canales, M.; Ramírez-de-Arellano, J.M.; Arellano, J.S.; Magaña, L.F. Ab Initio Study of the Interaction of a Graphene Surface Decorated with a Metal-Doped C₃₀ with Carbon Monoxide, Carbon Dioxide, Methane, and Ozone. *Int. J. Mol. Sci.* **2022**, *23*, 4933. <https://doi.org/10.3390/ijms23094933>

Academic Editor: Ana María Díez-Pascual

Received: 1 April 2022

Accepted: 21 April 2022

Published: 29 April 2022

Publisher's Note: MDPI stays neutral with regard to jurisdictional claims in published maps and institutional affiliations.



Copyright: © 2022 by the authors. Licensee MDPI, Basel, Switzerland. This article is an open access article distributed under the terms and conditions of the Creative Commons Attribution (CC BY) license (<https://creativecommons.org/licenses/by/4.0/>).

1. Introduction

Molecules, such as CO, CO₂, CH₄, and O₃, are air and water pollutants that threaten the environment and life, prompting the scientific community to develop technological solutions to such challenges [1–3]. In this study, we are interested in exploring the use of fullerenes for such aims.

Surfaces based on fullerenes and their variations have been widely studied since the prediction and further synthesis of the C₆₀ structure [4–6], a highly stable group of molecules consisting of 60 carbon atoms, also named buckminsterfullerene, buckyball, or simply fullerene. Although fullerenes, such as C₆₀, C₇₀, or larger, are the most commonly studied [7,8], smaller fullerenes can also be experimentally produced and are of particular interest due to their curvature [9–11].

Fullerene fragments such as a C₃₀ hydrocarbon—i.e., half of the buckminsterfullerene C₆₀—can show some of the properties of their complete counterparts [9] while also offering new possibilities due to their open basket-like shape. Similar nonplanar-related structures are corannulene (C₂₀H₁₀) and coronene, known since the 1960s [12–14]. The latter is a bowl carbon structure with 20 atoms or C₂₀, the smallest possible fullerene, which has been experimentally produced [11]. And the discovery of bidimensional, planar structures,

such as graphene [15,16] and borophene [17], has also attracted attention because of their attractive properties and potential applications.

Previous investigations from other authors considered fullerenes on a graphene surface, focusing on studying weak interactions at a molecular level [18]. Graphene can accept electrons from a C_{60} fullerene relatively quickly, which, combined with the high transport capability of the former, turns this hybrid material into a good candidate for solar cell technology [19]. The development of hybrid surfaces has also focused on fabricating graphene- C_{60} films on silicon surfaces by a multistep self-assembly process [20]. The potential applications of these systems are promising, especially as lubricating films in electromechanics microsystems. Graphene- C_{60} vertical heterostructures composed of C_{60} thin films have also focused on their structural and electrical properties [21]. The absorption of pollutants, such as $COCl_2$ (phosgene), H_2S , CO , or CO_2 , among others, by these hybrid structures has also raised attention. Decorating such arrangements with transition metals usually catalyzes absorption [22–25].

This work studies a mixed surface formed by a semifullerene C_{30} adsorbed on a defective 5×5 graphene layer without a hexagonal ring, i.e., six carbon vacancies. The roughness of the surface at several sites and the change in curvature make this an attractive system to dope with different atoms. We considered Li, Ti, and Pt-decorations and then studied the ability of the compound system to capture the pollutant molecules mentioned above. We found that all the molecules reacted with the surface except methane.

2. Results

2.1. Optimization of the Semifullerene C_{30}

We took two different parts when splitting a fullerene C_{60} into two halves (“bucky-balls”) [10] to obtain a semifullerene C_{30} . One has a pentagon in the base (section P), and the other has a hexagonal base (section H). Figure 1 shows the optimization for each case. Figure 1a,b show the C_{30} with a pentagon at the bottom, and Figure 1c,d show the C_{30} with a hexagonal base. After optimization, we discovered that in the C_{60} molecule, the separation between the carbon atoms is 1.425 Å. For section P, the distance is 1.444 Å at the bottom, and for the rest of the particles, the average separation is 1.375 Å. For section H, the space is 1.485 Å at the base, and the average spacing is 1.436 Å for the other particles. The results from other authors [10] agree with our results.

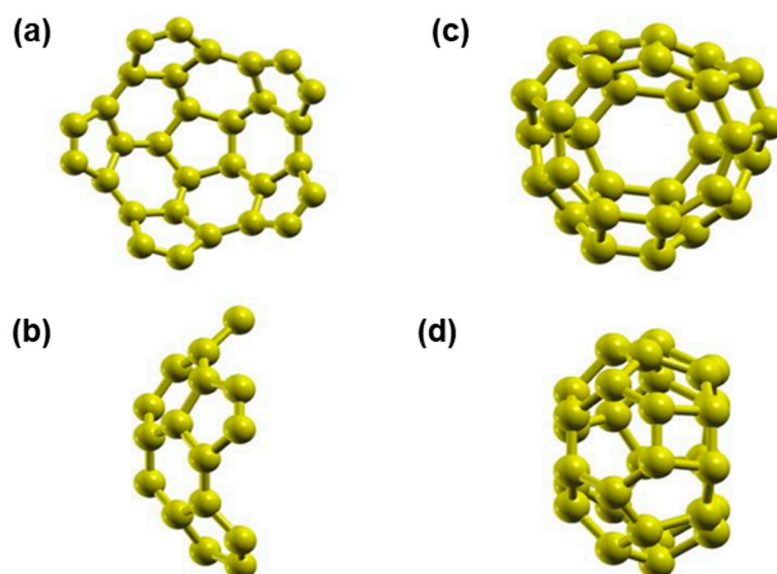


Figure 1. Molecules after optimization of C_{30} . In (a,b), we have C_{30} with a pentagonal base, in a front and a side view, respectively. In (c,d), we show a front and side view for C_{30} with a hexagonal base.

2.2. Optimization of Graphene with a Six-Vacancy Cluster

The vacancies in the graphene layer are necessary for the adsorption of the C₃₀ molecule. We considered a graphene unit cell with 50 atoms and made a six-vacancy cluster. Then, we optimized the system. Figure 2 shows the final configuration. We note that there is some distortion in the graphene lattice. The carbon atoms around the vacancies have different separations concerning pristine graphene. The bond lengths marked with A are 1.403 Å, and those marked with X are 1.452 Å. The other bonds are 1.420 Å, which is the same size as pristine graphene.

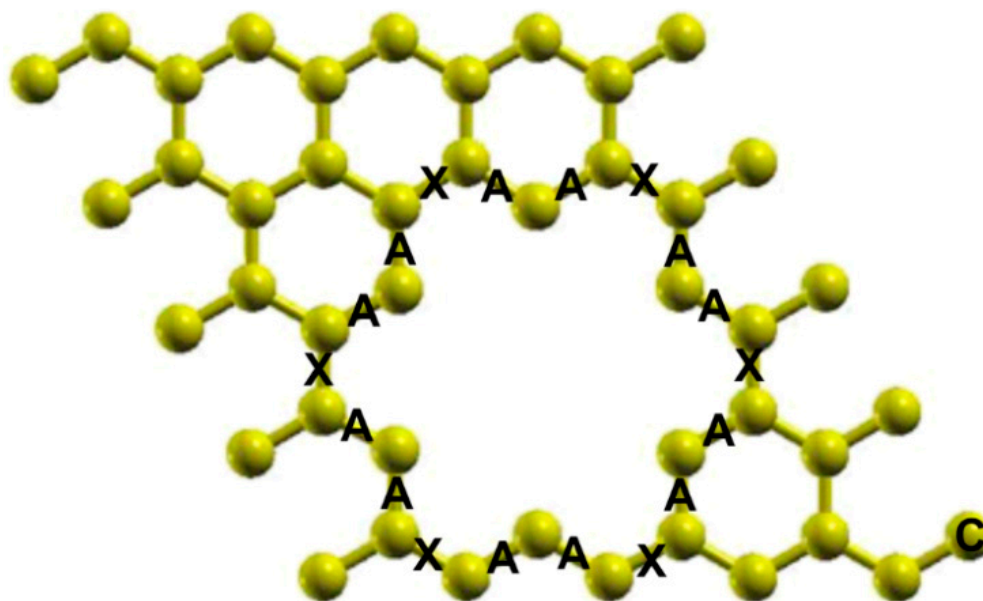


Figure 2. Unit cell after optimization of graphene with a six-vacancy cluster. The bond lengths marked with A are 1.403 Å, and those marked with X are 1.452 Å. The other bonds are the same size as in pristine graphene, 1.420 Å.

2.3. Adsorption of the C₃₀ Molecule with a Pentagonal Base

The left column (P) in Figure 3 shows the adsorption of the C₃₀ molecule with a pentagonal base in row 1. The initial location of the C₃₀ molecule is above the cluster vacancies. Besides, the molecule is, with the closest carbon atom to the surface, at a distance of 3 Å. In the same column, row 2, we can see the system's final configuration. The adsorption energy is −15.29 eV, indicating a powerful graphene reaction. We perceive a view from above, the graphene surface in row 3 of the same column after adsorption using four-unit cells.

2.4. Adsorption of the C₃₀ Molecule with a Hexagonal Base

Column H in row 1 shows the initial location of the C₃₀ molecule with a hexagonal bottom concerning the graphene layer with the closest carbon atom to the surface at a distance of 3 Å. In the same column, row 2, we can see the system's final configuration. The adsorption energy is −16.410 eV, which is a stronger adsorption than in the pentagonal case. We perceive the graphene surface in row 3 of the same column after adsorption using four-unit cells.

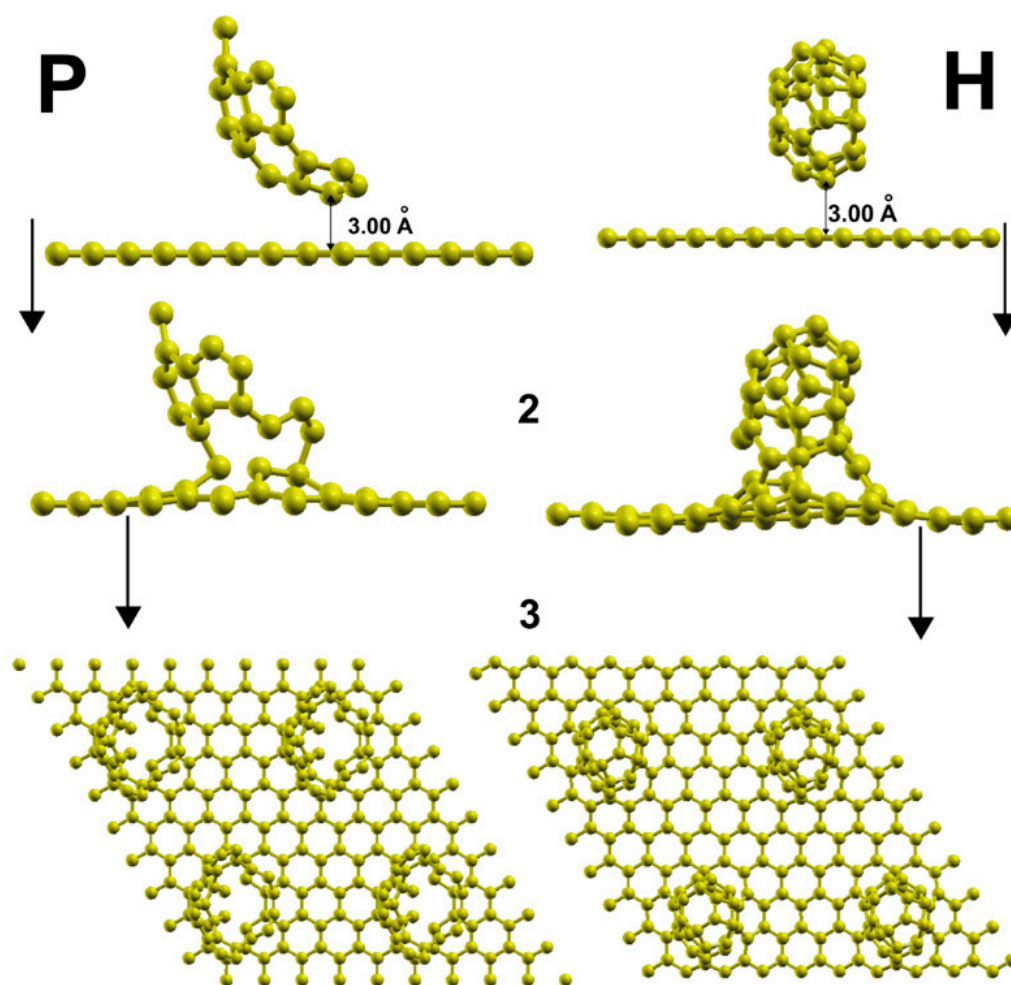


Figure 3. Adsorption of C_{30} on graphene with a six-vacancy cluster. In column P, we show the adsorption of the C_{30} molecule with a pentagonal base. In the same column P, in row 1, we have the initial location of the semifullerene. We have the final configuration after adsorption in the second row of the same column. We view the surface with four-unit cells from above in the last row of this column, P. The corresponding sequence for a C_{30} with a hexagonal base is in column H.

2.5. Adsorption of Metals on the Graphene- C_{30} (P) Surface

2.5.1. Doping with Li

Figure 4a presents the initial and final configuration for the adsorption of a lithium atom on the surface. The initial distance between the metal atom and the plane defined by the opening of C_{30} was 3.27 Å and 5.27 Å from the graphene layer. The lithium atom ends up bound to a carbon atom of the C_{30} . The adsorption energy of Li is -3.686 eV, which indicates a strong reaction with the surface. The Li atom yields 0.0561 electrons.

Figure 5 shows the interaction's projected density of states (PDOS). Note the hybridization of orbitals s and p from carbon with the orbital p from lithium around the Fermi energy at around 4 eV above the Fermi energy and about 2 eV below the Fermi energy.

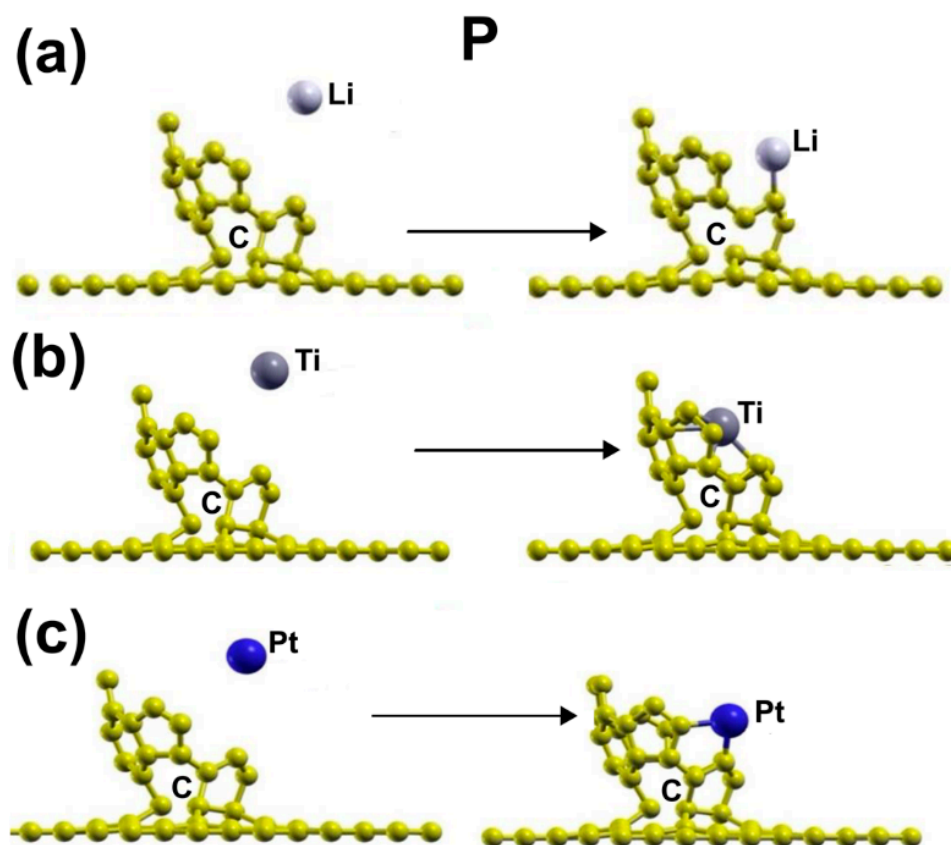


Figure 4. Adsorption of Li, Pt, and Ti on the graphene-C₃₀ system for the pentagonal base. The three metals adsorbed with a strong reaction on the surface. (a) presents the initial and final configuration for the adsorption of a lithium atom on the surface. (b) shows the initial and final configuration for the adsorption of a titanium atom on the surface. (c) shows the initial and final configuration for the adsorption of a platinum atom on the surface.

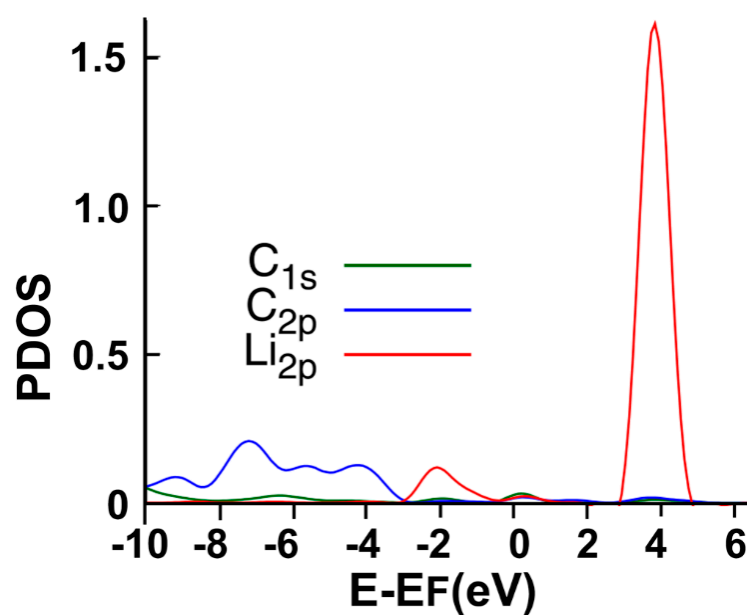


Figure 5. The PDOS for the adsorption of Li on the graphene-C₃₀ system for the pentagonal base.

2.5.2. Doping with Ti

Figure 4b shows the initial and final configuration for the adsorption of a titanium atom on the surface. The initial distance between the metal atom and the plane defined by the opening of C_{30} was 3.34 Å and 5.25 Å from the graphene layer. The titanium atom ends up bound to four carbon atoms of the C_{30} . The adsorption energy is -8.082 eV, implying an intense reaction. The Ti atom yields 0.6129 electrons to the surface.

We can see in Figure 6 the interaction's PDOS. We note the hybridization of orbitals s and d from titanium with the orbitals p from the neighboring carbon atoms between -4 eV, a bit below the Fermi energy, and between 1 eV and 5 eV.

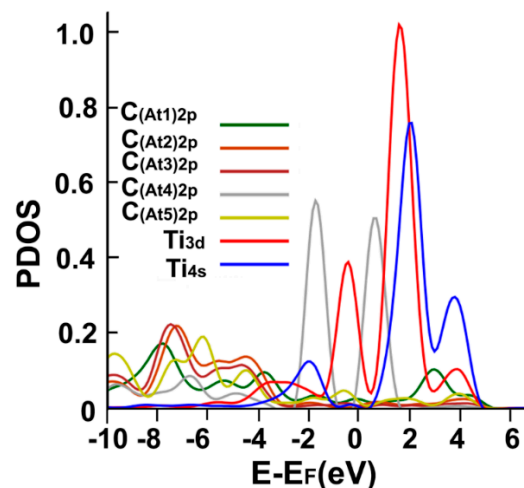


Figure 6. The PDOS for the adsorption of Ti on the graphene- C_{30} system for the pentagonal base.

2.5.3. Doping with Pt

Figure 4c shows the initial and final configuration for the adsorption of a platinum atom on the surface. The initial distance between the metal atom and the plane defined by the opening of C_{30} was 3.36 Å and 5.24 Å from the graphene layer. The platinum atom ends up bound to two carbon atoms of the C_{30} , with an adsorption energy of -5.982 eV, showing a strong reaction with the surface again. The Pt atom yields 0.3910 electrons to the surface.

Figure 7 shows the corresponding PDOS. We note the hybridization of orbital p from carbon with the orbitals s and p from platinum, around the Fermi energy, at around 2 eV above the Fermi energy, at about 2 eV below the Fermi energy, and below -4 eV.

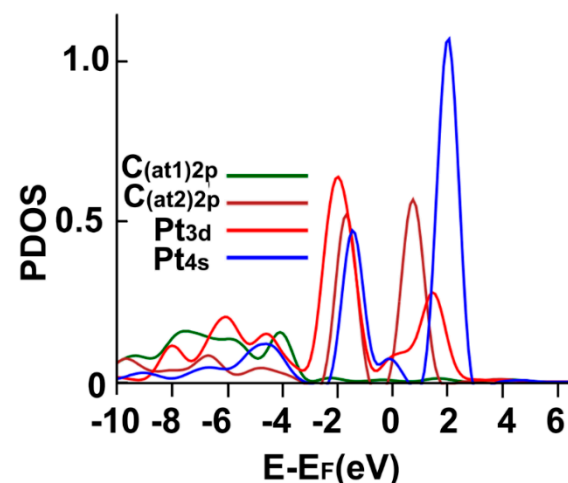


Figure 7. The PDOS for the adsorption of Pt on the graphene- C_{30} system for the pentagonal base.

2.6. Adsorption of Metals on the Graphene-C₃₀ (H) Surface

2.6.1. Doping with Li

Figure 8a shows the initial and final configuration for the adsorption of a lithium atom on the surface. The initial distance between the metal atom and the plane defined by the opening of C₃₀ was 3.37 Å and 4.57 Å from the graphene layer. The lithium atom ends up bound to a carbon atom of C₃₀ with an adsorption energy of −1.551 eV. It is a strong reaction but not as intense as the pentagonal case. The Li atom transfers 0.0364 electrons to the surface.

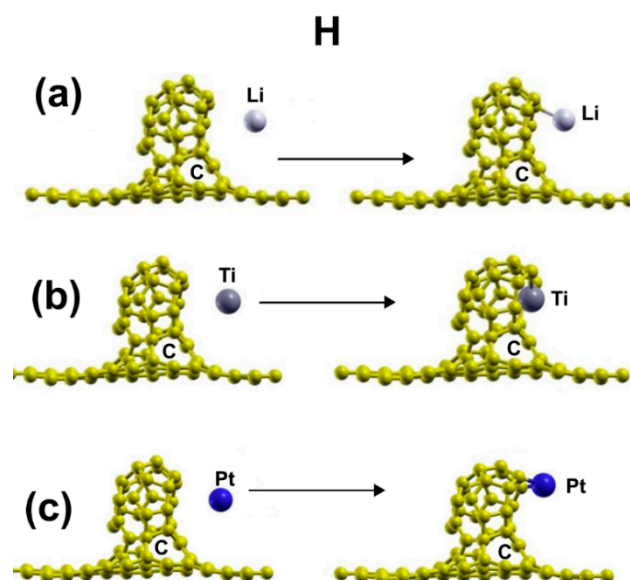


Figure 8. Adsorption of Li, Pt, and Ti on the graphene-C₃₀ system for the hexagonal base. The three metals adsorbed strongly. (a) shows the initial and final configuration for the adsorption of a lithium atom on the surface. (b) shows the initial and final configuration for the adsorption of a titanium atom on the surface. (c) presents the initial and final configuration for the adsorption of a platinum atom on the surface.

Figure 9 shows the interaction's PDOS. Note the hybridization of orbitals s and p from carbon with the orbital p from lithium, between 1eV and 3 eV, around 4 eV, and a weaker hybridization between −2 eV and −1 eV.

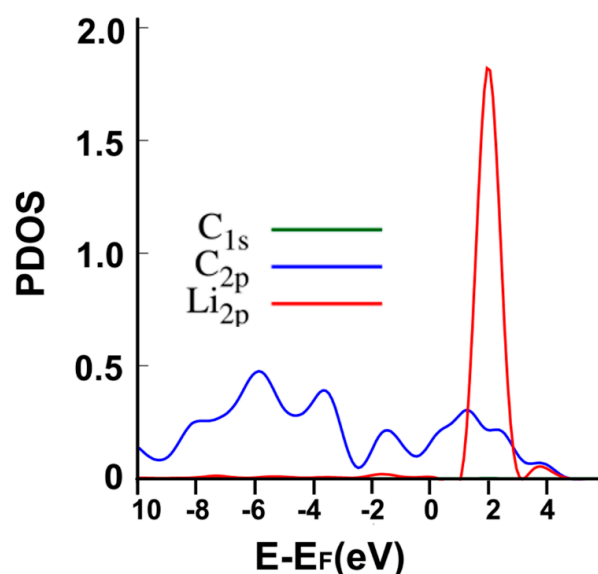


Figure 9. The PDOS for the adsorption of Li on the graphene-C₃₀ system for the hexagonal base.

2.6.2. Doping with Ti

Figure 8b shows the initial and final configuration for the adsorption of a titanium atom on the surface. The initial distance between the metal atom and the plane defined by the opening of C_{30} was 3.34 Å and 4.57 Å from the graphene layer. The titanium atom ends up bound to two carbon atoms of C_{30} . The adsorption energy of the titanium atom is -5.435 eV. The Ti atom transfers 0.6179 electrons to the system. The interaction is intense but not as much as in the pentagonal case.

We can see in Figure 10 the interaction's PDOS. We note the hybridization of orbitals s and d from titanium with the orbitals p from the neighboring carbon atoms around -2 eV and between the Fermi energy and 5 eV.

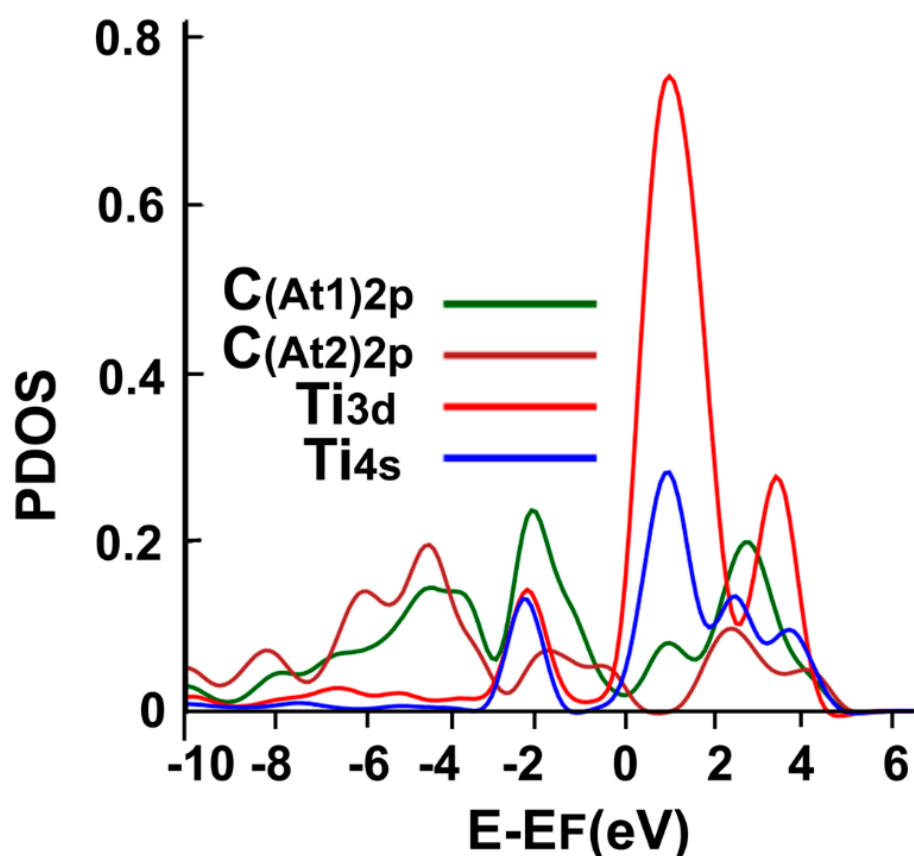


Figure 10. The PDOS for the adsorption of Ti on the graphene- C_{30} system for the hexagonal base.

2.6.3. Doping with Pt

Figure 8c presents the initial and final configuration for the adsorption of a platinum atom on the surface. The initial distance between the metal atom and the plane defined by the opening of C_{30} was 3.34 Å and 4.57 Å from the graphene layer. The platinum atom ends up bound to two carbon atoms of C_{30} . The adsorption energy of the platinum atom is -4.706 eV, which is a strong interaction with the surface but not as intense as in the pentagonal case.

The Pt atom transfers 0.5141 electrons to the surface. Figure 11 shows the corresponding PDOS. We note the hybridization of orbital p from carbon atoms with the orbitals s and d from platinum, at around -2 eV, about 1.5 eV, and below -4 eV.

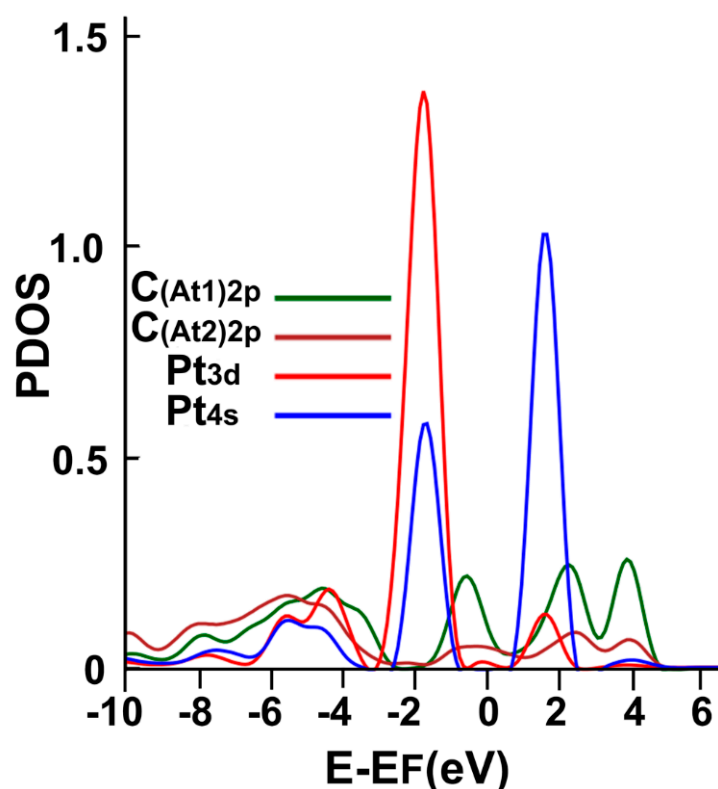


Figure 11. The PDOS for the adsorption of Pt on the graphene-C₃₀ system for the hexagonal base.

2.7. Adsorption of Pollutant Molecules on the Li-doped Graphene-C₃₀ (P) Surface

2.7.1. Adsorption of CO

There is no adsorption in this case.

2.7.2. Adsorption of CO₂

Figure 12a shows the initial and final configuration of the system for the adsorption of a carbon dioxide molecule. The molecule ends up bound to the lithium atom via the oxygen atom with an adsorption energy of -0.373 eV. The molecule transfers 0.04688 electrons to the surface.



Figure 12. (a) The adsorption of CO₂ on the Li-doped graphene-C₃₀ system for the pentagonal base. The initial distance between the carbon atom of the CO₂ molecule and the Li atom was 3.17 Å, and the distance from the graphene layer was 7.12 Å. The molecule was parallel to the graphene layer. The adsorption is without dissociation. (b) The PDOS for the adsorption of CO₂ on the Li-doped graphene-C₃₀ system for the pentagonal base.

Figure 12b shows the corresponding PDOS. We note the hybridization of orbital p from the oxygen atom with the orbital s from lithium at around 3 eV.

2.7.3. Adsorption of O₃

Figure 13a shows the initial and final configuration of the system for the adsorption of an ozone molecule. The molecule ends up bound to the lithium atom without dissociation.

The adsorption energy is -1.777 eV, and using MD at 300 K, we found that the particle Li-O₃ remains close to the surface at that temperature.

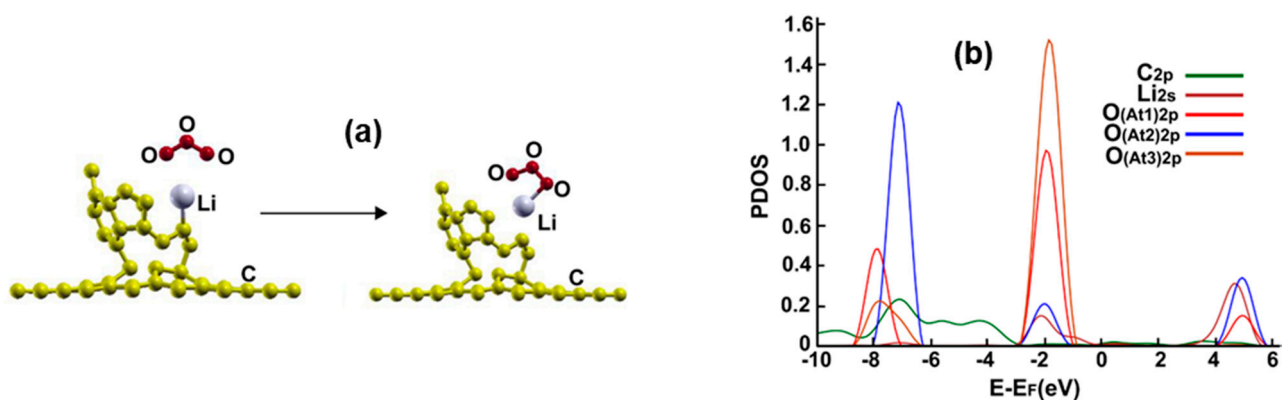


Figure 13. (a) The adsorption of O₃ on the Li-doped graphene-C₃₀ system for the pentagonal base. The initial distance between the central oxygen atom of the O₃ molecule and the Li atom was 3.015 Å, and the distance from the graphene layer was 7.15 Å. The molecule was perpendicular to the graphene layer. The adsorption is without dissociation. (b) The PDOS for the adsorption of O₃ on the Li-doped graphene-C₃₀ system for the pentagonal base.

Figure 13b shows the corresponding PDOS. Notice the weak hybridization of orbitals p from the oxygen and carbon atoms with the orbitals s from the lithium between 0 and 2 eV.

2.8. Adsorption of Pollutant Molecules on the Ti-Doped Graphene-C₃₀ (P) Surface

2.8.1. Adsorption of CO

Figure 14a shows the initial and final configuration of the system for the adsorption of a carbon monoxide molecule. The molecule ends up bound to the titanium atom without dissociation via the carbon atom. The adsorption energy is -1.21 eV, and the molecule gains 0.0322 electrons from the surface.

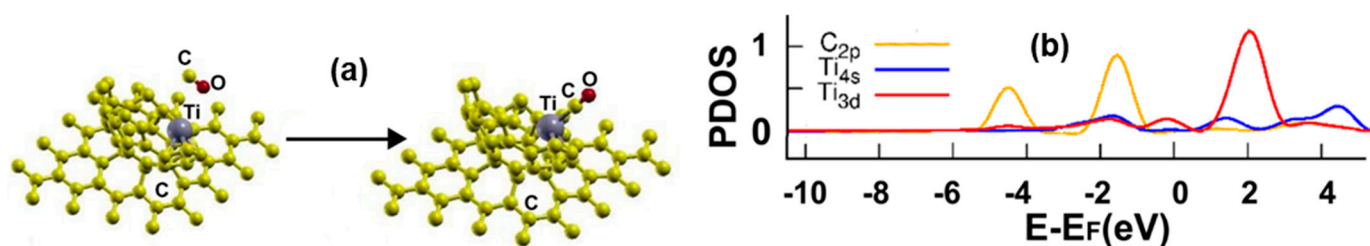


Figure 14. (a) Adsorption of CO on the Ti-doped graphene-C₃₀ system for the pentagonal base. The initial distance between the carbon atom of the CO molecule and the Ti atom was 4.18 Å, and the distance from the graphene layer was 7.34 Å. The molecule was parallel to the graphene layer. The adsorption is without dissociation. (b) The PDOS for the adsorption of CO on the Ti-doped graphene-C₃₀ system for the pentagonal base.

Figure 14b shows the corresponding PDOS. Notice the hybridization of orbital p from the carbon atom with the orbitals s and d from the titanium atom at around -2 eV and between 1 eV and 4 eV.

2.8.2. Adsorption of CO₂

There is no adsorption in this case.

2.8.3. Adsorption of CH₄

There is no adsorption in this case.

2.8.4. Adsorption of O₃

Figure 15a shows the initial and final configuration of the system for the adsorption of an ozone molecule. The molecule dissociates into an oxygen atom and an oxygen molecule. The oxygen atom is bound to the titanium, and the oxygen molecule is attached to the titanium atom. The adsorption energy of the ozone molecule is -6.3953 eV. The oxygen atom loses 0.2702 electrons. Besides, the oxygen molecule gains 0.4085 electrons. Using MD at 300 K, we obtained that the particle Ti-O₃ remains close to the surface at that temperature.

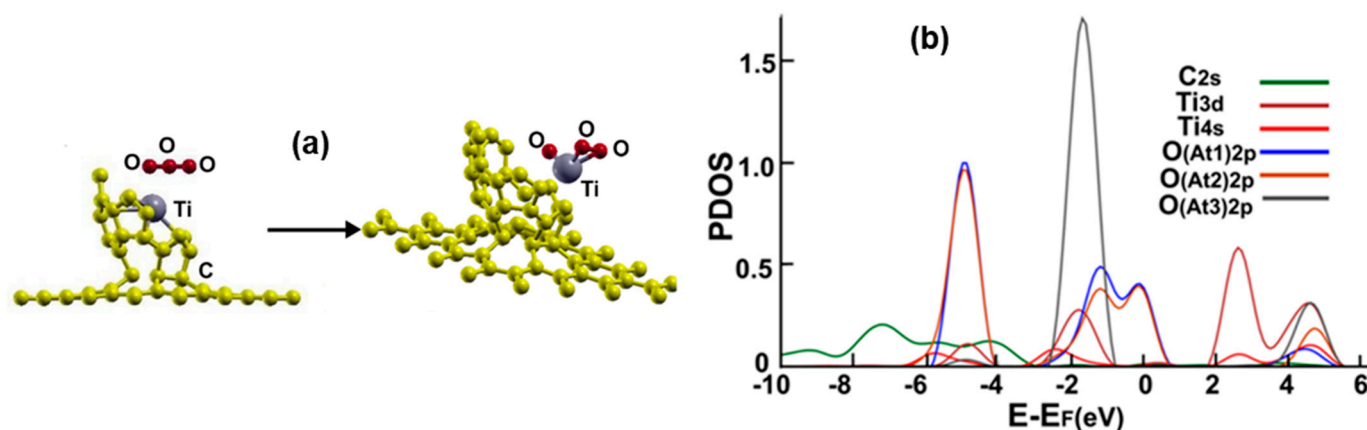


Figure 15. (a) Adsorption of O₃ on the Ti-doped graphene-C₃₀ system for the pentagonal base. The initial distance between the central oxygen atom and the Ti atom was 3.0 Å, and the distance from the graphene layer was 7.14 Å. The plane of the ozone molecule was parallel to the graphene layer. The adsorption is with dissociation. (b) The PDOS for the adsorption of O₃ on the Ti-doped graphene-C₃₀ system for the pentagonal base.

Figure 15b shows the corresponding PDOS. Notice a weak hybridization of orbitals s from the carbon atom with the orbitals s and d from the titanium atom and p orbitals from the oxygen atoms at around 4 eV and between -6 eV and -4 eV with p orbitals from oxygen atoms and orbitals s from the titanium atom.

2.9. Adsorption of Pollutant Molecules on the Pt-Doped Graphene-C₃₀ (P) Surface

2.9.1. Adsorption of CO

There is no adsorption in this case.

2.9.2. Adsorption of CO₂

There is no adsorption in this case.

2.9.3. Adsorption of CH₄

There is no adsorption in this case.

2.9.4. Adsorption of O₃

Figure 16a shows the initial and final configuration of the system for the adsorption of an ozone molecule. The adsorption energy is -0.8521 eV, and the molecule dissociates into an oxygen atom and an oxygen molecule. The oxygen atom ends up bound to a carbon atom. Besides, the oxygen molecule ends up bound to the platinum atom. The oxygen atom, which ends bound to a carbon atom, transfers 0.1207 electrons. The remaining part of the ozone molecule, the oxygen molecule bound to the Pt atom, gains 0.5665 electrons.

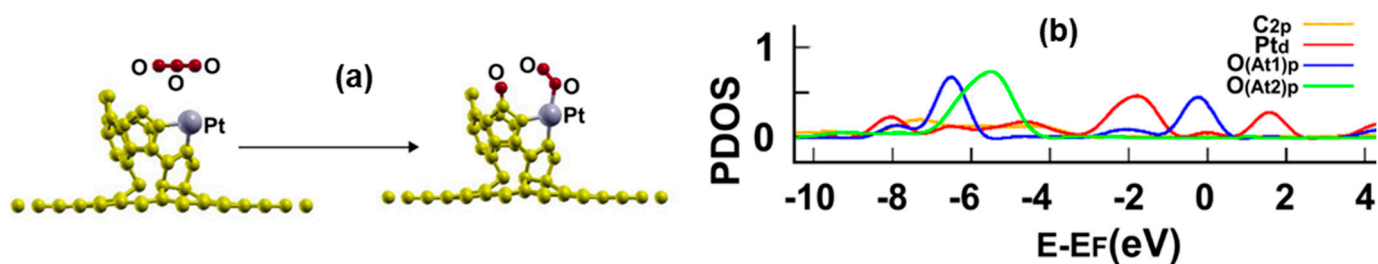


Figure 16. (a) Adsorption of O_3 on the Pt-doped graphene- C_{30} system for the pentagonal base. The initial distance between the central oxygen atom and the Pt atom was 3.60 \AA , and the distance from the graphene layer was 7.25 \AA . The plane of the ozone molecule was parallel to the graphene layer. The adsorption is with dissociation. (b) The PDOS for the adsorption of O_3 on the Pt-doped graphene- C_{30} system for the pentagonal base.

Figure 16b shows the corresponding PDOS. Notice a weak hybridization of orbitals p from the carbon atom with the orbitals p from the platinum and oxygen atoms at around 4.2 eV . The same hybridization is stronger below -4 eV .

2.10. Adsorption of Pollutant Molecules on the Li-Doped Graphene- C_{30} (H) Surface

2.10.1. Adsorption of CO

There is no adsorption in this case.

2.10.2. Adsorption of CO_2

Figure 17a shows the initial and final configuration of the system for the adsorption of a carbon dioxide molecule. The molecule adsorbs without dissociation, and one oxygen atom ends up bound to the lithium atom. The adsorption energy is -0.6491 eV , and the molecule transfers to the system 0.0803 electrons. The calculated recovery time at 300 K is 0.13 s , a good value for a sensor.

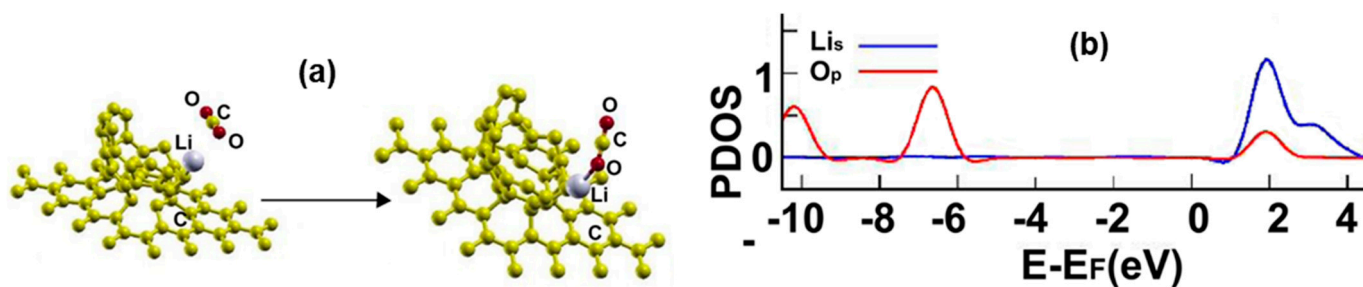


Figure 17. (a) Adsorption of CO_2 on the Li-doped graphene- C_{30} system for the hexagonal base. The initial distance between the carbon atom of the CO_2 molecule and the Li atom was 3.11 \AA , and the distance from the graphene layer was 7.15 \AA . The molecule was parallel to the graphene layer. The adsorption is without dissociation. (b) The PDOS for the adsorption of CO_2 on the Li-doped graphene- C_{30} system for the hexagonal base.

Figure 17b shows the corresponding PDOS. Notice the hybridization of orbitals p from the oxygen atom with the orbitals s from the lithium atom at around 2 eV .

2.10.3. Adsorption of CH_4

There is no adsorption in this case.

2.10.4. Adsorption of O_3

Figure 18a shows the initial and final configuration of the system for the adsorption of an ozone molecule. The molecule ends up bound to the lithium atom without dissociation. The adsorption energy of the ozone molecule is -2.119 eV , and the surface transfers

0.2883 electrons to the ozone molecule. Using MD at 300 K, we found that the particle Li-O₃ remains close to the surface at that temperature; it does not go away from the surface.

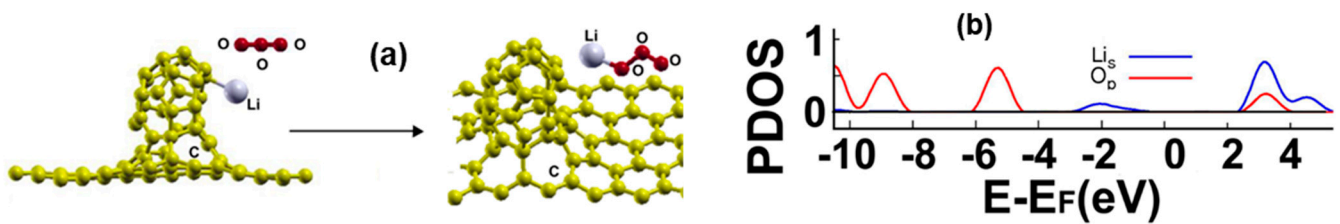


Figure 18. (a) Adsorption of O₃ on the Li-doped graphene-C₃₀ system for the hexagonal base. The initial distance between the central oxygen atom and the Li atom was 3.26 Å, and the distance from the graphene layer was 7.35 Å. The plane of the ozone molecule was parallel to the graphene layer. The adsorption is without dissociation. (b) The PDOS for the adsorption of O₃ on the Li-doped graphene-C₃₀ system for the hexagonal base.

Figure 18b shows the corresponding PDOS. Notice the hybridization of orbitals p from the oxygen with the orbitals s from the lithium atom between 3 eV and 4 eV. There is a weaker hybridization below the Fermi energy.

2.11. Adsorption of Pollutant Molecules on the Ti-Doped Graphene-C₃₀ (H) Surface

2.11.1. Adsorption of CO

There is no adsorption in this case.

2.11.2. Adsorption of CO₂

There is no adsorption in this case.

2.11.3. Adsorption of CH₄

There is no adsorption in this case.

2.11.4. Adsorption of O₃

Figure 19a shows the initial and final configuration of the system for the adsorption of an ozone molecule. The adsorption energy is -0.8214 eV, and the molecule dissociates into two fractions during adsorption, an oxygen atom and an oxygen molecule. Besides, the first fraction is bound to a carbon atom, and the second remains close to the surface. Using MD at 300 K, we found that the molecule O₂ remains close to the surface at that temperature; it does not go away from the surface.

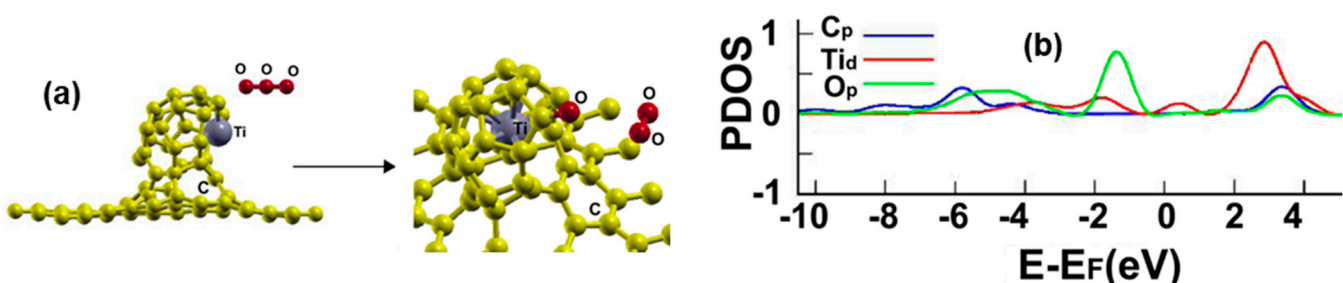


Figure 19. (a) Adsorption of O₃ on the Ti-doped graphene-C₃₀ system for the hexagonal base. The initial distance between the central oxygen atom and the Ti atom was 3.97 Å, and the distance from the graphene layer was 6.90 Å. The plane of the ozone molecule was parallel to the graphene layer. The adsorption is with dissociation into an oxygen atom and an oxygen molecule. (b) The PDOS for the adsorption of O₃ on the Ti-doped graphene-C₃₀ system for the hexagonal base.

Figure 19b shows the corresponding PDOS. Notice the hybridization of orbitals p from the carbon and oxygen atoms and the orbitals d from the titanium atom between 2 and 4 eV and below the Fermi energy.

2.12. Adsorption of Pollutant Molecules on the Pt-Doped Graphene-C₃₀ (H) Surface

2.12.1. Adsorption of CO

Figure 20a shows the initial and final configuration of the system for the adsorption of a carbon monoxide molecule. The adsorption energy is -1.756 eV without dissociation. The carbon atom ends up bound to the platinum atom.

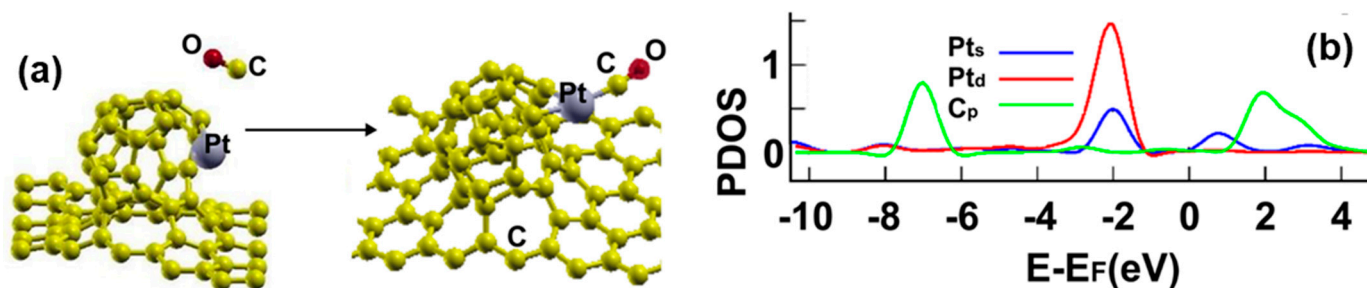


Figure 20. (a) Adsorption of CO on the Pt-doped graphene-C₃₀ system for the hexagonal base. The initial distance between the center of the CO molecule and the Pt atom was 3.0 Å, and the distance from the graphene layer was 7.32 Å. The molecule was parallel to the graphene layer. The adsorption is without dissociation; (b) The PDOS for the adsorption of CO on the Pt-doped graphene-C₃₀ system for the hexagonal base.

The surface transfers 0.0322 electrons to the carbon monoxide molecule. Figure 20b shows the corresponding PDOS. We can see the hybridization of orbitals p from the carbon atom and the orbitals s from the platinum atom at around 3 eV and about 1.2 eV, respectively. We can also notice a weak hybridization of orbitals p from the carbon atom with orbitals d and s from the platinum atom below -1 eV.

2.12.2. Adsorption of CO₂

There is no adsorption in this case.

2.12.3. Adsorption of CH₄

There is no adsorption in this case.

2.12.4. Adsorption of O₃

Figure 21a shows the initial and final configuration of the system for the adsorption of an ozone molecule that occurs with dissociation and with an adsorption energy of -1.43 eV. The molecule splits into two parts, an oxygen atom and an oxygen molecule. Using MD at 300 K, we found that the particle O₂ remains close to the surface at that temperature; it does not go away from the surface.

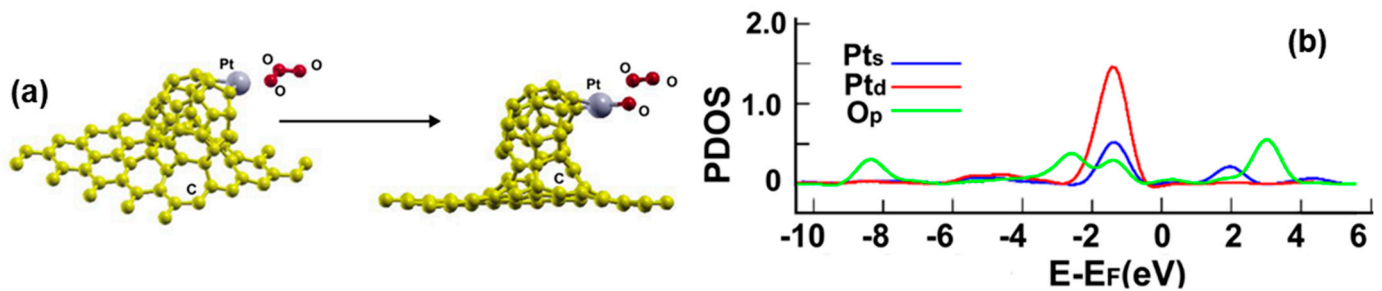


Figure 21. (a) Adsorption of O₃ on the Pt-doped graphene-C₃₀ system for the hexagonal base. The initial distance between the central oxygen atom and the Pt atom was 3.18 Å, and the distance from the graphene layer was 7.21 Å. The plane of the ozone molecule was parallel to the graphene layer. The adsorption is with dissociation. (b) The PDOS for the adsorption of O₃ on the Pt-doped graphene-C₃₀ system for the hexagonal base.

The oxygen atom, which ends bound to the platinum atom, transfers 0.1207 electrons. The surface transfers 0.5665 electrons to the remaining fraction of the ozone molecule and the oxygen molecule, which remains close to the surface.

Figure 21b shows the corresponding PDOS. We can see the hybridization of orbitals p from the oxygen atom and the orbitals s and d from the platinum atom at around 2 eV and about −1.75 eV, respectively. We can also notice a weak hybridization of orbitals p from the oxygen atom with orbitals d and s from the platinum atom below −2 eV.

3. Materials and Methods

We used the GGA approximation for the exchange and correlation energies in the Perdew–Burke–Ernzerhof (PBE) expression [26], using a Martins–Troullier norm-conserving pseudopotential [27]. We performed structural relaxations using the Quantum ESPRESSO code package [28], which uses periodical boundary conditions. We took threshold energy of 1.0×10^{-6} eV for convergence, a cut-off energy point of 1100 eV, and a threshold force of 1.0×10^{-5} eV/Å. We considered 40 k points within the Monkhorst–Pack particular k point scheme for Brillouin-zone integrations [29] with a separation of 0.083 \AA^{-1} .

To check the pseudopotentials, we minimized the energy of the different systems. Thus, we obtained the Li lattice parameter 3.495 Å (the experimental value is 3.510 Å) [30]; for titanium, we obtained: $a = 2.863 \text{ \AA}$, and $c = 4.544 \text{ \AA}$ (the observed values are 2.950 and 4.683 Å, respectively [30]; in the case of Pt, we calculated a lattice parameter of 2.898 Å (the experimental value is 2.924 Å). We obtained the bond lengths and angles of the different pollutant molecules we are considering with the same approach. Figure 22 shows our results, which agree with the experimental values.

In our simulations, the adsorption energy is:

$$E_{ads} = E(Surf + Mol) - [E(Surf) + E(Mol)], \quad (1)$$

where $E(Surf + Mol)$ is the energy corresponding to the final system; $[E(Surf) + E(Mol)]$ corresponds to the initial configuration, which is the energy of the surface, without interaction with the molecule plus the isolated molecule's energy.

We calculated the recovery time (τ) from the Eyring transition state theory using the expression [31,32]:

$$\tau = [h / (k_B T)] e^{-E_{ads} / (k_B T)} \quad (2)$$

In Equation (2), h is the Planck's constant, k_B is the Boltzmann's constant, E_{ads} is the adsorption energy, and T is the absolute temperature.

The desirable set of values for the recovery time is between 10^{-2} and ten seconds, implying at 300 K, adsorption energies in the range (−0.6428, −0.8215) eV.

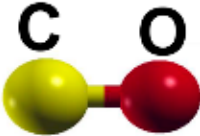
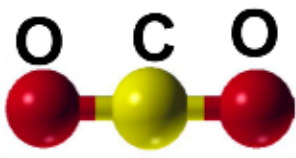
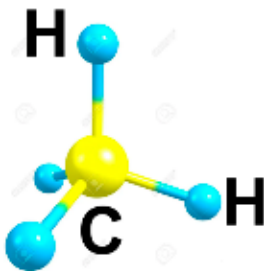
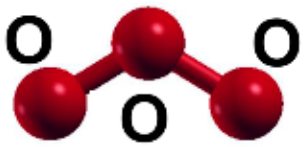
	<p>carbon monoxide Bond length: 1.287 Å (1.299 Å)</p>
	<p>carbon dioxide Bond length C-O: 1.152 Å (1.162 Å) angle O-C-O: 179.960° (180°)</p>
	<p>methane Bond length C-H: 1.087 Å (1.090 Å) angle O-C-O: 109.760° (109.500°)</p>
	<p>ozone Bond length: 1.276 Å (1.278 Å) angle O-O-O : 118.635° (116.780°)</p>

Figure 22. We compare our results, obtained by minimizing the molecule energy, and the experimental values are given in parenthesis.

4. Discussion

We performed computational simulations to investigate the adsorption of polluting molecules on graphene-semifullerene (C_{30}) surfaces, considering two C_{30} geometries: hexagonal and pentagonal base. We found it possible to dope all surfaces with the metals Li, Ti, and Pt, which we used as catalysts in the adsorption of the different polluting molecules. We consider as pollutant molecules CO, CO₂, CH₄, and O₃.

We obtained the semifullerene adsorbs on the graphene surface with adsorption energies of -14.97 eV and -16.41 eV, respectively, for pentagonal and hexagonal bases. The adsorption occurs on a six-vacancy cluster in a graphene layer. Besides, the catalysts adsorb on the graphene- C_{30} surface with a pentagonal base with adsorption energies of -4.02 eV, -6.3 eV, and -8.4 eV for Li, Pt, and Ti, respectively. For the hexagonal base, the adsorption energies are -1.87 eV, -4.7 eV, and -5.43 eV, in the same order. Notice that in each case (P or H), Li shows the adsorption energy with the minor magnitude and Ti with the largest.

The carbon monoxide molecule adsorbs on the pentagonal-base (P) surface only when Ti is the dopant, with an adsorption energy of -3.6 eV, and this adsorption is without dissociation. Furthermore, CO adsorbs on the hexagonal-base (H) surface only with Pt as the dopant with an adsorption energy of -0.89 eV. Again, the adsorption is without dissociation.

The carbon dioxide molecule adsorbs on both surfaces but only with Li as the dopant, with adsorption energies of: -0.67 eV for the P surface and -0.54 eV for the H surface. The adsorption of the CO₂ molecule is without dissociation.

The methane molecule did not adsorb on any surface.

Finally, we found that both surfaces always adsorb the ozone molecule. When Ti or Pt are dopants, we found that the O₃ molecule always dissociates into an oxygen molecule and an oxygen atom. For the P surface, the adsorption energies are -6.3953 and -0.8521 eV for the Ti and Pt doped surfaces, respectively. Furthermore, the adsorption energies for the Ti and Pt doped H surface are -0.82 eV and -1.43 eV, respectively. In the case of Li, the O₃ molecule adsorbs without dissociation. The adsorption energy is -1.777 eV for the P surface, and the adsorption energy is -2.119 eV for the H surface.

At 300 K, the P surface would not act as a suitable sensor in any case. The H surface would be a sensor for O₃ with Ti as the dopant ($\tau = 9.97$ s) and for CO₂ with Li as a dopant ($\tau = 0.13$ s).

Author Contributions: Conceptualization, methodology, validation, formal analysis, investigation, M.C., J.S.A., and L.F.M.; resources, L.F.M.; data curation, M.C. and J.M.R.-d.-A.; writing—original draft preparation, writing—review and editing, M.C., J.M.R.-d.-A., J.S.A., and L.F.M.; project administration, funding acquisition, L.F.M. All authors have read and agreed to the published version of the manuscript.

Funding: This research was funded by Dirección General de Asuntos del Personal Académico de la Universidad Nacional Autónoma de México, grant number IN113220. The APC was funded by Tecnológico de Monterrey.

Institutional Review Board Statement: Not applicable.

Informed Consent Statement: Not applicable.

Data Availability Statement: Not applicable.

Acknowledgments: We thank Dirección General de Asuntos del Personal Académico de la Universidad Nacional Autónoma de México, partial financial support by Grant IN-111817. We also appreciate UNAM-Miztli-Super-Computing Center technical assistance by the project LANCAD-UNAM-DGTIC-030, and the Yoltila (UAM-Iztapalapa) computer facilities. M. C. acknowledges CONACYT for a scholarship during this research.

Conflicts of Interest: The authors declare no conflict of interest.

References

1. Kjellstrom, T.; Lodh, M.; McMichael, T.; Ranmuthugala, G.; Shrestha, R.; Kingsland, S. Air and Water Pollution: Burden and Strategies for Control. In *Disease Control Priorities in Developing Countries*; Jamison, D.T., Breman, J.G., Measham, A.R., Alleyne, G., Claeson, M., Evans, D.B., Jha, P., Mills, A., Musgrove, P., Eds.; World Bank: Washington, DC, USA, 2006; ISBN 978-0-8213-6179-5.
2. World Health Organization Don't Pollute My Future! The Impact of the Environment on Children's Health. Available online: <https://www.who.int/publications-detail-redirect/WHO-FWC-IHE-17.01> (accessed on 12 April 2022).
3. Hussain, A.; Rehman, F.; Rafeeq, H.; Waqas, M.; Asghar, A.; Afsheen, N.; Rahdar, A.; Bilal, M.; Iqbal, H.M.N. In-Situ, Ex-Situ, and Nano-Remediation Strategies to Treat Polluted Soil, Water, and Air—A Review. *Chemosphere* **2022**, *289*, 133252. [[CrossRef](#)]
4. Osawa, E. Superaromaticity. *Kagaku* **1970**, *25*, 854–863.
5. Kroto, H.W.; Heath, J.R.; O'Brien, S.C.; Curl, R.F.; Smalley, R.E. C₆₀: Buckminsterfullerene. *Nature* **1985**, *318*, 162–163. [[CrossRef](#)]
6. Sygula, A. Chemistry on a Half-Shell: Synthesis and Derivatization of Buckybowls. *Eur. J. Org. Chem.* **2011**, *2011*, 1611–1625. [[CrossRef](#)]
7. Astefanei, A.; Núñez, O.; Galceran, M.T. Characterisation and Determination of Fullerenes: A Critical Review. *Anal. Chim. Acta* **2015**, *882*, 1–21. [[CrossRef](#)]
8. Murayama, H.; Tomonoh, S.; Alford, J.M.; Karpuk, M.E. Fullerene Production in Tons and More: From Science to Industry. *Fuller. Nanotub. Carbon Nanostruct.* **2005**, *12*, 1–9. [[CrossRef](#)]
9. Rabideau, P.W.; Abdourazak, A.H.; Folsom, H.E.; Marcinow, Z.; Sygula, A.; Sygula, R. Buckybowls: Synthesis and Ab Initio Calculated Structure of the First Semibuckminsterfullerene. *J. Am. Chem. Soc.* **1994**, *116*, 7891–7892. [[CrossRef](#)]
10. Rabideau, P.W.; Sygula, A. Buckybowls: Polynuclear Aromatic Hydrocarbons Related to the Buckminsterfullerene Surface. *Acc. Chem. Res.* **1996**, *29*, 235–242. [[CrossRef](#)]
11. Prinzbach, H.; Weiler, A.; Landenberger, P.; Wahl, F.; Wörth, J.; Scott, L.T.; Gelmont, M.; Olevano, D. Gas-Phase Production and Photoelectron Spectroscopy of the Smallest Fullerene, C₂₀. *Nature* **2000**, *407*, 60–63. [[CrossRef](#)]
12. Barth, W.E.; Lawton, R.G. Dibenzo[Ghi,Mno]Fluoranthene. *J. Am. Chem. Soc.* **1966**, *88*, 380–381. [[CrossRef](#)]
13. Lawton, R.G.; Barth, W.E. Synthesis of Corannulene. *J. Am. Chem. Soc.* **1971**, *93*, 1730–1745. [[CrossRef](#)]

14. Filatov, A.S.; Petrukhina, M.A. Probing the Binding Sites and Coordination Limits of Buckybowls in a Solvent-Free Environment: Experimental and Theoretical Assessment. *Coord. Chem. Rev.* **2010**, *254*, 2234–2246. [[CrossRef](#)]
15. Meyer, J.C.; Geim, A.K.; Katsnelson, M.I.; Novoselov, K.S.; Booth, T.J.; Roth, S. The Structure of Suspended Graphene Sheets. *Nature* **2007**, *446*, 60–63. [[CrossRef](#)] [[PubMed](#)]
16. Geim, A.K.; Novoselov, K.S. The Rise of Graphene. *Nat. Mater.* **2007**, *6*, 183–191. [[CrossRef](#)] [[PubMed](#)]
17. Boustani, I. New Quasi-Planar Surfaces of Bare Boron. *Surf. Sci.* **1997**, *370*, 355–363. [[CrossRef](#)]
18. Švec, M.; Merino, P.; Dappe, Y.J.; González, C.; Abad, E.; Jelínek, P.; Martín-Gago, J.A. Van Der Waals Interactions Mediating the Cohesion of Fullerenes on Graphene. *Phys. Rev. B* **2012**, *86*, 121407. [[CrossRef](#)]
19. Zhang, X.; Huang, Y.; Wang, Y.; Ma, Y.; Liu, Z.; Chen, Y. Synthesis and Characterization of a Graphene–C60 Hybrid Material. *Carbon* **2009**, *47*, 334–337. [[CrossRef](#)]
20. Pu, J.; Mo, Y.; Wan, S.; Wang, L. Fabrication of Novel Graphene–Fullerene Hybrid Lubricating Films Based on Self-Assembly for MEMS Applications. *Chem. Commun.* **2013**, *50*, 469–471. [[CrossRef](#)] [[PubMed](#)]
21. Kim, K.; Lee, T.H.; Santos, E.J.G.; Jo, P.S.; Salleo, A.; Nishi, Y.; Bao, Z. Structural and Electrical Investigation of C₆₀–Graphene Vertical Heterostructures. *ACS Nano* **2015**, *9*, 5922–5928. [[CrossRef](#)] [[PubMed](#)]
22. Zhang, T.; Sun, H.; Wang, F.; Zhang, W.; Tang, S.; Ma, J.; Gong, H.; Zhang, J. Adsorption of Phosgene Molecule on the Transition Metal-Doped Graphene: First Principles Calculations. *Appl. Surf. Sci.* **2017**, *425*, 340–350. [[CrossRef](#)]
23. Khodadadi, Z. Evaluation of H₂S Sensing Characteristics of Metals–Doped Graphene and Metals-Decorated Graphene: Insights from DFT Study. *Phys. E Low-Dimens. Syst. Nanostructures* **2018**, *99*, 261–268. [[CrossRef](#)]
24. Promthong, N.; Tabtimsai, C.; Rakrai, W.; Wannoo, B. Transition Metal-Doped Graphene Nanoflakes for CO and CO₂ Storage and Sensing Applications: A DFT Study. *Struct. Chem.* **2020**, *31*, 2237–2247. [[CrossRef](#)]
25. Khan, A.A.; Ahmad, I.; Ahmad, R. Influence of Electric Field on CO₂ Removal by P-Doped C₆₀-Fullerene: A DFT Study. *Chem. Phys. Lett.* **2020**, *742*, 137155. [[CrossRef](#)]
26. Perdew, J.P.; Burke, K.; Ernzerhof, M. Generalized Gradient Approximation Made Simple. *Phys. Rev. Lett.* **1997**, *78*, 1396. [[CrossRef](#)]
27. Kleinman, L.; Bylander, D.M. Efficacious Form for Model Pseudopotentials. *Phys. Rev. Lett.* **1982**, *48*, 1425–1428. [[CrossRef](#)]
28. Giannozzi, P.; Andreussi, O.; Brumme, T.; Bunau, O.; Buongiorno Nardelli, M.; Calandra, M.; Car, R.; Cavazzoni, C.; Ceresoli, D.; Cococcioni, M.; et al. Advanced Capabilities for Materials Modelling with Quantum ESPRESSO. *J. Phys. Condens. Matter* **2017**, *29*, 465901. [[CrossRef](#)] [[PubMed](#)]
29. Monkhorst, H.J.; Pack, J.D. Special Points for Brillouin-Zone Integrations. *Phys. Rev. B* **1976**, *13*, 5188–5192. [[CrossRef](#)]
30. Lide, D.R. (Ed.) *CRC Handbook of Chemistry and Physics: A Ready-Reference Book of Chemical and Physical Data*, 81st ed.; CRC Press: Boca Raton, FL, USA, 2000; ISBN 978-0-8493-0481-1.
31. Eyring, H. The Activated Complex in Chemical Reactions. *J. Chem. Phys.* **1935**, *3*, 107–115. [[CrossRef](#)]
32. Popa, I.; Fernández, J.M.; Garcia-Manyes, S. Direct Quantification of the Attempt Frequency Determining the Mechanical Unfolding of Ubiquitin Protein. *J. Biol. Chem.* **2011**, *286*, 31072–31079. [[CrossRef](#)]